The analysis of thermoelectric powder compaction mechanisms within field-activated sintering of skutterudites and Heusler alloys

© A.S. Tukmakova[1], N.I. Khakhilev[1], D.B. Shcheglova[1], V.D. Nasonov[1], A.P. Novitskii[2], I.A. Serhiienko[2], A.V. Novotelnova[1]

[1] ITMO University,
197101 St. Petersburg, Russia
[2] National University of Science and Technology MISiS,
119049 Moscow, Russia

E-mail: astukmakova@itmo.ru, daria.shcheglova1998@gmail.com

Received August 12, 2021
Revised August 28, 2021
Accepted August 28, 2021

The analysis of the shrinkage rate of powders, based on the power-law creep model of a porous body, was carried out in this paper to calculate the compaction parameters of $CoSb_3$-based skutterudites and Fe_2VAl-based Heusler alloys within field-activated sintering. It was indicated that this method, which had already been used for metal and ceramic powders, is applicable for thermoelectric powders. The values of strain rate sensitivity were obtained, and the corresponding powder compaction mechanisms have been defined. The main creep mechanism for skutterudites was found to be a dislocation climb, that later was replaced by grain boundary sliding, and the last sintering stage was associated with diffusional creep. The main creep mechanism for Heusler alloys was grain boundary sliding, later replaced by diffusional creep.

Keywords: field-assisted sintering, numerical simulation, powders compaction, skutterudites, Heusler alloys, thermoelectrics.

DOI: 10.21883/SC.2022.14.53886.10

1. Introduction

The thermoelectric figure of merit of a material depends to a considerable extent on the thermal conductivity, which may be reduced in bulk nanostructured materials. The most efficient way to produce such material structures is field-assisted sintering (FAS) that involves applying external uniaxial pressure to a nanopowder and passing pulsed alternating or direct current through it [1]. This ensures the generation of Joule heat, heating, and compaction of a powder. The resulting structure of the compacted material defines its future thermoelectric properties.

Two types of data need to be taken into account in the analysis of the FAS process: (1) technological parameters and (2) data on the sample microstructure (e.g., grain-size prior to sintering or the grain size after sintering). The technological parameters (temperature, heating rate, pressure, current, and reduction of the sample height) are monitored throughout the entire process. In contrast, the sample structure may be examined only before or after the process. A powder before sintering is characterized by its grain-size, bulk density, and X-ray diffraction analysis data. The structure of the sample after sintering is characterized by its porosity (or relative density), grain size, the phase composition variation, the presence of secondary recrystallization regions, parameters of grain boundaries and dislocations, etc.

Data on the variation of microstructure of the material in the course of powder compaction are hard to obtain experimentally and are needed to gain a complete understanding of the FAS process. The sintering kinetics pattern may be reconstructed by analyzing the sample shrinkage rate (time derivative of porosity) [2] with the use of the model of power-law creep of a porous body [3]. The key idea behind this approach is that numerical estimation of the powder shrinkage rate provides an opportunity to identify the compaction mechanisms: various types of motion of dislocations, grains, or diffusion processes.

A number of studies focused on the compaction of ceramic nanopowders have been published. For example, Wei et al. [2] examined the process of shrinkage of a ZrC powder under FAS at temperatures of 1650−2100°C. It was found that grain boundary sliding and dislocation glide-controlled creep were the primary compaction mechanisms. Lee et al. studied the mechanisms of ZrN compaction under FAS and high-voltage electric discharge consolidation [4]. It was demonstrated that dislocation climb-controlled creep is the dominant mechanism of compaction under FAS. However, the mechanism changed to diffusional creep after the application of a high electric voltage. Dislocation glide-controlled creep was identified as the key mechanisms of ZrN compaction under FAS [5], while dislocation climb-controlled creep was prevalent in hot pressing at the same temperature and pressure. The nature of the primary compaction mechanism depends on the sintering temperature and the applied pressure. For example, grain boundary sliding was the prevalent mechanism in a B_4C powder [6] at temperatures up to 2000°C and pressures up to 40 MPa, while dislocation climb-controlled creep became dominant at temperatures above 2000°C and pressures above 40 MPa.

The mechanisms of compaction of metal nanopowders under FAS have also been studied relatively thoroughly. The temperature and pressure dependences of the primary compaction mechanism for Ta were found to be similar to those for B_4C [7]. It was demonstrated that the primary mechanism changes from grain boundary diffusion to dislocation climb-controlled creep as the temperature increases. In TiAl [8], the primary compaction mechanism is dislocation climb-controlled creep accompanied by Al diffusion, and dislocation glide-controlled creep is significant only at the initial stage of shrinkage.

The power-law creep equation modified to include the effect of electromigration in the process of sintering of a metallic tungsten powder was used by Deng et al. [9]. It was demonstrated that the activation energy of power-law creep may be reduced by increasing the current density. The compaction process was also divided tentatively into two stages: at lower pressures, the primary compaction mechanism is grain boundary diffusion, while the key mechanism at higher pressures is dislocation climb-controlled creep coupled with grain boundary diffusion. A slightly different approach was used in the study performed by Yang et al. [10], where the shrinkage of a powder was characterized in terms of surface energy, mean size of particles, and powder viscosity. Relying on these parameters, the authors distinguished three compaction stages: shrinkage controlled by the surface energy, defects of the crystal lattice, and high-temperature creep.

Since all the published studies were concerned with powders of metallic and ceramic materials, a question arises as to whether this approach is applicable in the analysis of sintering of semiconductor thermoelectric powders with varying properties. In the present study, the chosen approach is applied to two groups of medium-temperature thermoelectrics: Heusler alloys based on Fe_2VAl and skutterudites based on $CoSb_3$. The aim of it is to verify the feasibility of application of this approach in the analysis of kinetics of sintering of thermoelectric powders.

2. Analysis of the shrinkage rate of powders with the use of the model of power-law creep of a porous body

Relying on the power-law creep equation [11] and considering a porous body subjected to external pressure, Olevsky has derived the following governing equation for explicit characterization of the stress-strain state in the process of sintering of porous materials [12]:

$$\sigma_{ij} = A_{cr} W^{m-1} \left[\varphi \dot{\varepsilon}_{ij} + \left(\psi - \frac{1}{3} \varphi \right) \dot{e} \delta_{ij} \right] + P_L \delta_{ij}, \quad (1)$$

where σ_{ij} is the external pressure; W is the equivalent effective strain rate that depends on porosity θ, rates of shape and volume change $\dot{e}$, and shear φ and bulk ψ moduli; P_L is the effective sintering stress and δ_{ij} is the Kronecker delta ($\delta_{ij} = 1$ if $i = j$, $\delta_{ij} = 0$ if $i \neq j$); the last term in Eq. (1) may be neglected in the case of field-activated sintering; $\dot{\varepsilon}_{ij}$ is the strain rate; and A_{cr} is the creep coefficient depending on coefficient A_m that is a complex material parameter:

$$A_{cr} = A_m T^m \exp\left(\frac{mQ}{RT} \right), \quad (2)$$

where T is temperature, m is the sensitivity to the strain rate, Q is the activation energy of power-law creep, and R is the gas constant.

The following equation was obtained using Eq. (1) [2]:

$$\dot{\theta} = \frac{d\theta}{dt} = -\left(\frac{\sigma_z}{A_m T^m \exp\left(\frac{mQ}{RT}\right)} \right)^{\frac{1}{m}} \left(\frac{3\theta}{2} \right)^{\frac{m+1}{2m}} (1-\theta)^{\frac{m-3}{2m}}, \quad (3)$$

where σ_z is the applied axial stress and $\dot{\theta}$ is the porosity change rate.

The following creep mechanisms are distinguished depending on the temperature and the pressure applied [13]:

– dislocation creep, which is subdivided into dislocation glide (motion of dislocations in a certain crystallographic direction) and dislocation climb (crossing of obstacles or vacancies by dislocations);

– diffusional creep — crystal strain induced by the diffusion of vacancies in the lattice, which results in plastic straining of a material;

– grain boundary sliding/grain boundary diffusion, which consists in mutual displacement of grains at a low strain rate and a high temperature.

The dominant creep mechanism is defined by the value of coefficient n or reciprocal coefficient m of sensitivity to the strain rate [1]. The analysis of sintering kinetics based on Eq. (3) then comes down to finding the value of coefficient m. Different creep mechanisms are characterized by the following values of m:

– $m = 1$, $n = 1$ — diffusion creep, which is also called Nabarro–Herring creep;

– $m = 0.5$, $n = 2$ — grain boundary sliding creep proposed by Gifkins;

– $m = 0.33$, $n = 3$ — dislocation glide-controlled creep presented by Weertman;

– $m = 0.22 - 0.33$, $n = 3 - 5$ — dislocation climb-controlled creep, which was also characterized by Weertman.

The process of nanopowder compaction depends not only on coefficient m, but also on coefficients A_m and Q in formula (3). The theoretical estimation or calculation of these coefficients is by no means a trivial task; in most studies, Q is determined using the graphical analytic method [6–8], and A_m, which characterizes the material microstructure, is considered to remain constant throughout the entire process [4], is adjusted [2] (using various methods of adjustment of coefficients of a function with

a known value), or is not calculated at all. All three coefficients are adjusted in the present study using the generalized descending gradient method, but the focus is on parameter m: in the case in point, it varies throughout the process of sintering and thus allows one to monitor the gradual interchange of primary compaction mechanisms.

3. Analysis of the shrinkage rate of powders of Heusler alloys based on Fe_2VAl and skutterudites based on $CoSb_3$

The shrinkage rate of powders was analyzed using six samples of different compositions based on Heusler alloys $Fe_2V_{1-x}Nb_xAl_{1-y}Ga_y$, where $x = y = 0$, 0.1, 0.2 (Table 1), and seven samples of skutterudites of the $Ga_xIn_yTe_zCo_4Sb_{12}$ nominal composition, where $x = y = 0$, 1 and $z = 0$, 0.5, 1, 2, 3 (Table 2).

A Dr. Sinter-1080 SPS (Fuji-SPS, Japan) spark plasma sintering setup was used to sinter samples of Heusler alloys and skutterudites. Powders for sintering were introduced into a cylindrical graphite mold with an internal diameter of 15 mm, and external diameter of 35 mm, and a height of 50 mm. Carbonized paper was inserted between the sample material, punches, and the mold. The pressure was 50 MPa for samples based on Fe_2VAl and 56 MPa for $CoSb_3$-based skutterudites. The pressure was kept constant for all samples throughout the entire process up to the end of exposure to the sintering temperature; after that, the pressure was reduced gradually to ~ 10 MPa. The heating rate of all samples was 50°/min (for Heusler alloys, it was monitored using a pyrometer; heating was performed manually to a temperature of 573°C at a rate no higher than 50°/min), and the cooling rate was not monitored. The sintering temperature of skutterudites was 650°C, and they were exposed to it for 10 min; the corresponding values for Heusler alloys were 1060°C and 5 min. The produced voltage and the current passed through the mold were set automatically, but did not exceed 1.5 V and 1000 A for all samples, respectively.

The so-called sintering maps (i.e., time dependences of temperature, pressure (force), current passed through the graphite mold, voltage, vacuum level in the working chamber, and extent and rate of compaction (shrinkage) of the sample material determined based on the displacement of the upper electrode) were recorded continuously in the process of sintering. A thermocouple inserted into a special hole in the mold was used for temperature measurements; the distance between the hole bottom and the sample

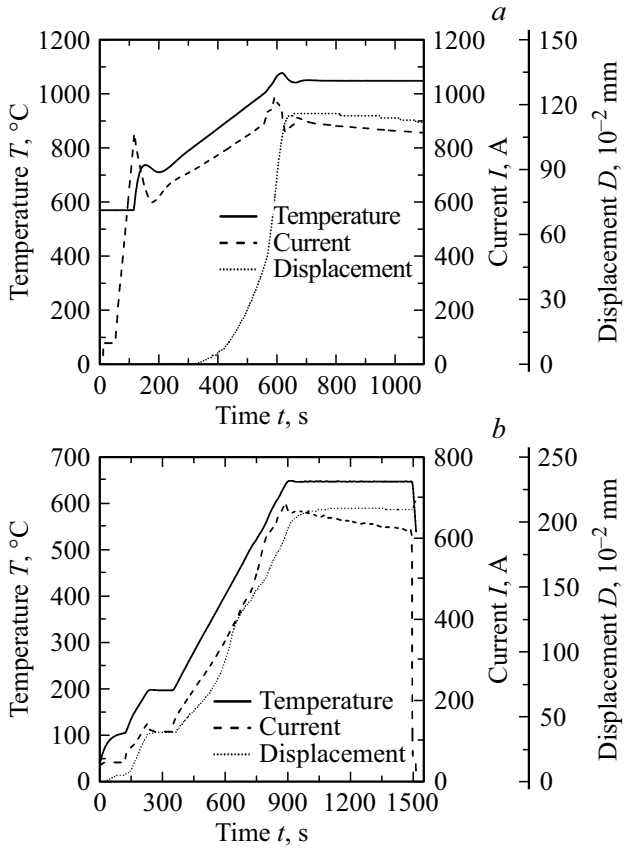

Figure 1. Time dependences of temperature, current, and shrinkage typical of (a) Heusler alloys and (b) skutterudites

Table 1. Nominal composition, mass before sintering m_{st}, mold diameter d_m, density after sintering ρ_{end}, and height of samples before (h_0) and after (h_{end}) sintering of Heusler alloys $Fe_2V_{1-x}Nb_xAl_{1-y}Ga_y$ ($x = y = 0$, 0.1, 0.2)

Nominal composition	m_{st}, g	d_m, mm	ρ_{end}, g/cm^3	h_{end}, mm	h_0, mm
$Fe_2V_{0.9}Nb_{0.1}Al$	3.11	15	6.50	2.70	3.14
$Fe_2V_{0.8}Nb_{0.2}Al$	1.53		6.50	1.33	2.47
$Fe_2VAl_{0.9}Ga_{0.1}$	2.05		6.61	1.76	2.38
$Fe_2VAl_{0.8}Ga_{0.2}$	1.60		6.55	1.38	2.33
$Fe_2V_{0.9}Nb_{0.1}Al_{0.9}Ga_{0.1}$	1.58		6.84	1.31	2.61
$Fe_2V_{0.8}$ $Nb_{0.2}A_{l0.8}Ga_{0.2}$	2.19		6.95	1.78	2.34

Table 2. Nominal composition, mass before sintering m_{st}, mold diameter d_m, density after sintering ρ_{end}, and height of samples before (h_0) and after (h_{end}) sintering of skutterudites $Ga_xIn_yTe_zCo_4Sb_{12}$ ($x = y = 0$, 1, $z = 0$, 0.5, 1, 2, 3)

Nominal composition	m_{st}, g	d_m, mm	ρ_{end}, g/cm^3	h_{end}, mm	h_0, mm
$GaInCo_4Sb_{12}Te_3$	4	15	7.52	3.01	6.43
$GaInCo_4Sb_{12}Te_1$			7.52	3.01	4.55
$CoSb_3$			7.56	2.99	4.14
$GaCo_4Sb_{12}Te_1$			7.48	3.03	4.45
$GaCo_4Sb_{12}Te_2$			7.34	3.08	4.42
$GaCo_4Sb_{12}Te_3$			7.57	2.99	5.16
$InCo_4Sb_{12}Te_3$			7.62	2.97	4.97

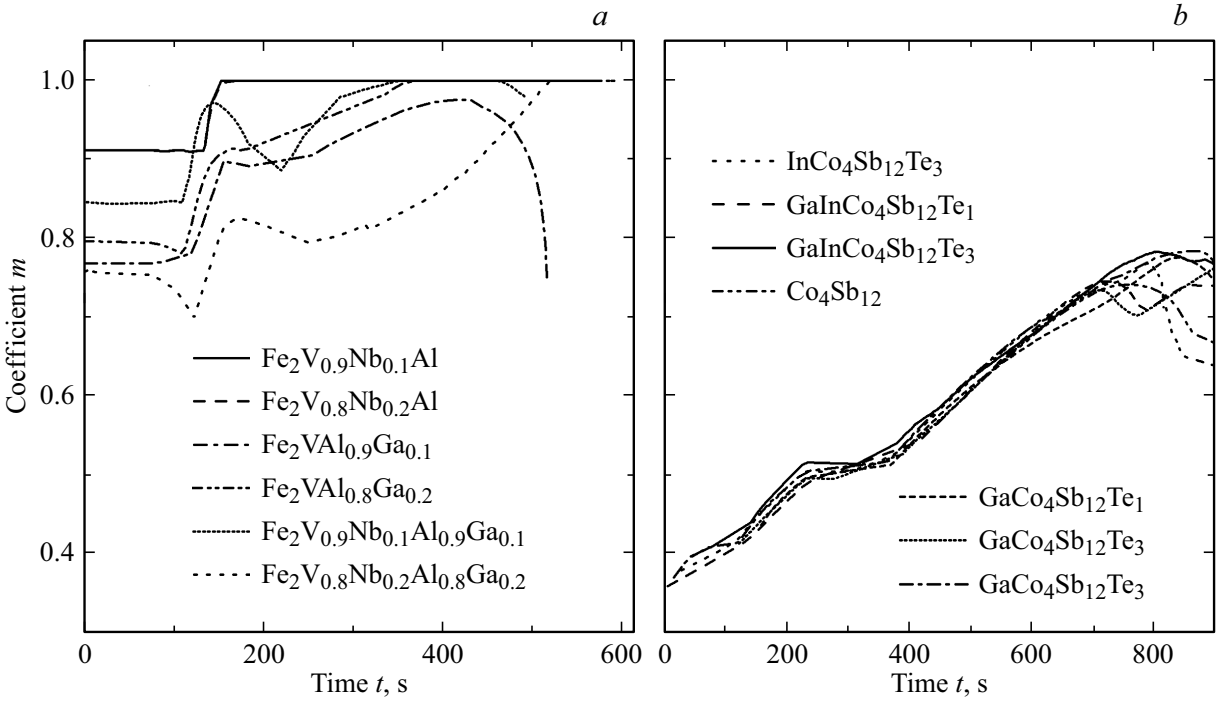

Figure 2. Dependences of coefficient m on the sintering time for (a) Heusler alloys $Fe_2V_{1-x}Nb_xAl_{1-y}Ga_y$ ($x = y = 0$, 0.1, 0.2) and (b) skutterudites $Ga_xIn_yTe_zCo_4Sb_{12}$ ($x = y = 0$, 1, $z = 0$, 1, 2, 3)

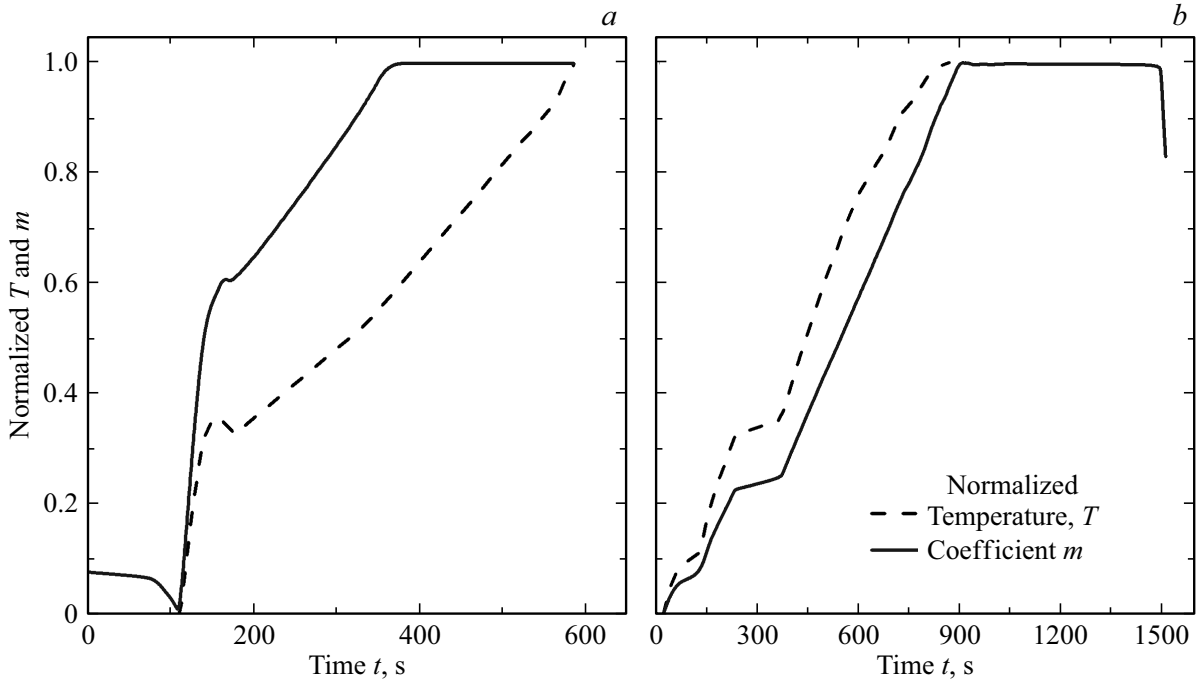

Figure 3. Normalized values of coefficient m and temperature for (a) $Fe_2VAl_{0.8}Ga_{0.2}$ and (b) $GaInCo_4Sb_{12}Te_3$

surface was no greater than 1 mm. Figure 1 shows the time dependences of temperature, current, pressure, and shrinkage values typical of Heusler alloys and skutterudites.

The calculation of parameters characterizing microprocesses in the sample was carried out in MS Excel. This was done by writing down function (3) (time derivative of porosity) for several time points with a pitch of approximately 50–100 s, which depended on the sample. At each time point, instantaneous values of the sintering temperature, applied pressure, and porosity were inserted

into function $d\theta/dt$. The instantaneous porosity values were calculated based on the instantaneous values of shrinkage and sample volume. The values of parameters Q and m, which act as coefficients of this function, were then adjusted. Having found the solution, we obtained optimized values of A_m, m, and Q.

4. Results

Plots of variation of coefficient m of sensitivity to the strain rate with sintering time t were obtained for samples of Heusler alloys and skutterudites (Fig. 2).

In the case of Heusler alloys, the values of m varied from ~ 0.75 to ~ 0.91 at the start of the experiment and reached a constant value within the range of 0.97–1 as sintering proceeded further. This corresponds to the transition from the grain boundary sliding mechanism to diffusion processes (Fig. 2, *a*).

Three compaction stages may be distinguished for skutterudites (Fig. 2, *b*):

1. dislocation glide-controlled creep is prevalent at $0.35 < m < 0.4$;

2. at $0.4 < m < 0.5$, the primary strain mechanism changes gradually to grain boundary sliding;

3. at the final stage ($0.5 < m < 0.8$), the diffusion creep mechanism is dominant.

5. Discussion

The results of comparison of the obtained m values for Heusler alloys and skutterudites suggest that the shrinkage mechanisms of samples differ. Parameter m for skutterudites assumes lower values (from 0.35 to 0.8) and varies in a wider range than the corresponding parameter for Heusler alloys (their m varies from 0.75 to 1). This may be attributed to the difference in mechanical properties of materials and the higher ductility of Heusler alloys. These alloys also feature higher coefficients of thermal and electric conductivity; this may translate into faster heating of powders and facilitate diffusion.

The dependence of parameter m on the sintering time is similar in nature to the time dependence of the sintering temperature. Figure 3 shows the normalized dependences of temperature and parameter m on the sintering time for one skutterudite sample and one Heusler alloy sample. The same correspondence was observed for all the other samples of different compositions.

Thus, one possible approach to controlling the interchange of compaction mechanisms involves the adjustment of sample heating rate in the process of sintering. If necessary, the heating rate curve may be modified so as to maintain a specific preferable sintering mechanism or adjust the time of operation of a certain mechanism. In order to do that, one needs to identify the compaction mechanism active at the initial stage of sintering (which should remain unchanged in samples of the same composition processed under the same pressure). The results of calculations carried out for samples processed at different heating rates and different sintering temperatures are required to gain a more complete understanding of the relation between functions $m(t)$ and $T(t)$.

At the initial time, parameter m for samples of Heusler alloys assumes different values. Since the temperature at this instant is equal to room temperature and current does not run through the sample due to its high porosity, it may be concluded that the initial value of m depends on pressure and the characteristics of the studied nanopowder. Therefore, powders of different initial grain-size compositions processed under different pressures should be considered separately.

6. Conclusion

It was demonstrated that the kinetics of sintering of thermoelectric powders may be analyzed using the model of power-law creep of a porous body. In implementing this approach, a power-law approximation of the time derivative of porosity and subsequent analysis of the function with the use of the generalized descending gradient method are expedient. The approach allows one to monitor variations of the power exponent of the function and associate them with specific prevalent mechanisms of powder compaction.

Funding

The experiments in this study (sintering of skutterudites) were supported by a grant from the Russian Science Foundation (project No. 19-79-10282). The simulation work was supported financially by the ITMO University.

Conflict of interest

The authors declare that they have no conflict of interest.

References

[1] O. Guillon, J. Gonzalez Julian, B. Dargatz, T. Kessel, G. Schierning, J. Räthel, M. Herrmann. Adv. Eng. Mater., **16** (7), 830 (2014).

[2] X. Wei, C. Back, O. Izhvanov, O.L. Khasanov, C.D. Haines, E.A. Olevsky. Materials, **8** (9), 6043 (2015).

[3] D.V. Dudina, B.B. Bokhonov, E.A. Olevsky. Materials, **12** (3), 541 (2019).

[4] G. Lee, M.S. Yurlova, D. Giuntini, E.G. Grigoryev, O.L. Khasanov, J. McKittrick, E.A. Olevsky. Ceram. Int., **41** (10), 14973 (2015).

[5] G. Lee, E.A. Olevsky, C. Manière, A. Maximenko, O. Izhvanov, C. Back, J. McKittrick. Acta Mater., **144**, 524 (2018).

[6] M. Zhang, T. Yuan, R. Li, S. Xie, M. Wang, Q. Weng. Ceram. Int., **44** (4), 3571 (2018).

[7] C. Dong, X. Bi, J. Yu, R. Liu, Q. Zhang. J. Alloys Compd., **781**, 84 (2019).

[8] Z. Trzaska, G. Bonnefont, G. Fantozzi, J.P. Monchoux. Acta Mater., **135**, 1 (2017).
[9] S. Deng, R. Li, T. Yuan, S. Xie, M. Zhang, K. Zhou, P. Cao. Scripta Mater., **143**, 25 (2018).
[10] C. Yang, M.D. Zhu, X. Luo, L.H. Liu, W.W. Zhang, Y. Long, E.J. Lavernia. Scripta Mater., **139**, 96 (2017).
[11] F.R. Nabarro. Mater. Sci. Eng. A-struct., **387**, 659 (2004).
[12] E.A. Olevsky. Mater. Sci. Eng. R. **23** (2), 41 (1998).
[13] K.R. Athul, U.T.S. Pillai, A. Srinivasan, B.C. Pai. Adv. Eng. Mater., **18** (5), 770 (2016).